CHAPTER 9

The Simulation of Large-Scale Neural Networks

MATTHEW A. WILSON and JAMES M. BOWER

9.1 Introduction

Previous chapters have described techniques used to simulate the responses of single neurons in isolation to different patterns of inputs by modeling their detailed biophysical structure. In the brain, it is the anatomical and physiological characteristics of the complex neural circuits in which single neurons are embedded that determine the actual pattern of inputs to a cell as well as the significance of the cell's output. As with single isolated cells, computer simulations can provide a means to study the complex functional relationships between neurons comprising such networks (see chapters 6, 7 and 8).

Traditionally, most models of brain circuitry have focused on simulating the macroscopic or "higher-order" functionality of systems of simplified computational or neuronal units. In fact, the prevalence of models of this type has made the modeling of neural networks, in general, synonymous with an abstracted treatment of neural processing in which the study of function takes precedence over the details of implementation. Periodic attempts have been made over the last twenty years to develop neural network models that are structurally more realistic (Pellionisz, Llinas, and Perkel 1977). However, we would argue that only recently have technical developments made simulations of realistic, large-scale neural networks truly practical. One of these technical developments is the rapid increase in affordable computational power, which allows the simulation of models with considerable complexity. Equally important for this kind of modeling is the increasing sophistication of neurophysiological and neuroanatomical techniques, which has resulted in an explosive growth in the availability of structural details on which this type of modeling relies.

In this chapter we will consider the construction and simulation of neural network models that are fundamentally based on the anatomical

structure and physiological characteristics of actual biological networks. We have found, through our own modeling efforts, that this "structural" approach to modeling has several distinct advantages over strictly abstract treatments (Wilson and Bower 1988). First, biological realism allows known neuroanatomical and neurophysiological data to be used to constrain the values of many model parameters. This limits the parameter space of a model that needs to be explored to tune and characterize the behavior of complex network models. Second, biologically accurate simulations can more readily generate neuronal-like outputs comparable to data from actual physiological experiments. This increases the likelihood that predictions of the models will be relevant and testable. For example, our models generate intracellular membrane potentials, single-spike output, and extracellular field potentials (fig. 9.7; Wilson and Bower, 1980). And finally, models closely based on the structural properties of biological networks force functional hypotheses to fit within the physical constraints imposed by the actual biological system. In this way insights provided by this type of detailed modeling provide directions for more abstracted studies while at the same time assuring their relevance to actual network properties (Wilson and Bower 1988).

While structural simulations can provide a means to study the functional properties of complex networks, they are also potentially valuable to experimental neurobiology. In particular, simulations that are based on a biological system often highlight undescribed but important features of the modeled networks and thus can suggest important network or cellular parameters to characterize experimentally. This experimental/modeling interaction is especially important given the powerful experimental tools that are currently available to neurobiologists and the wide range of data that they can generate. Thus, this type of structural modeling provides a framework in which detailed experimental data can be organized and interpreted, and biologically relevant theories of brain function can be studied.

9.2 Network Modeling Considerations

Having stated the general advantages of structural neural network models, and made the claim that the revolution in computing power and neurophysiological and neuroanatomical data has made them more accessible, it is important to point out explicitly that the process of modeling still requires working within considerable limitations. In fact, even with the tremendous increases in available computing power, no existing

computer can practically simulate all that is known about large neural networks, while at the same time no neural structure has yet been described in all its structural detail. Even in so-called simpler invertebrate networks, experimentalists are well aware that a vast amount of information relevant to function must still be extracted, yet modelers are still forced to simplify their networks for simulation purposes (see chapters 6 and 7). The main body of this chapter outlines our approach to these issues by describing a model of the piriform (olfactory) cortex in some detail. However, we will first consider more specifically some of the general technical factors involved in designing and implementing such a model given these limitations.

Faced with both incomplete information about the networks to be modeled and insufficient computing power to incorporate all information that is currently known, the major task in simulating large-scale, realistic networks is determining the appropriate modeling approximations. In most cases the basic test of the appropriateness of these approximations in structural models will be whether the simulated network can replicate fundamental (and measurable) behavior of the actual system. Of course, as the sophistication of the questions asked with a simulation increases so does the necessary complexity of the model. As such, the process of network modeling can be seen as a bootstrap operation that ideally goes hand in hand with experimental work. To discuss this general relationship between model complexity and simulation objectives we will consider two levels of structural organization at which approximations are often made, the cellular level and the network level.

9.2.1 Cellular Complexity

In modeling single cells, there are several types of structural details to consider. There is spatial/cellular structure, which includes characteristics such as dimension, extent, and location of cell bodies, dendrites, axons, and spines. Then there is biophysical/subcellular structure with membranes, channels, receptors, and their voltage- and time-dependent characteristics including channel conductances, membrane resistance and capacitance, the nature of receptor binding, ionic diffusion, and buffering. Previous chapters have shown that these features can be modeled in some detail if that is the primary objective. However, the network modeler must determine the relative benefit of including such details given the computational cost. Again, it is the nature of the questions asked that determines which details are most critical. For example, in our simulations of the piriform cortex the spike output of a cell is not modeled using a complete Hodgkin-Huxley model for ac-

tion potentials; instead, a simple threshold criterion is applied to the membrane potential to generate discrete spike events. The occurrence of these spikes is indicated with a spike waveform "pasted" onto the actual membrane potential at the appropriate time. In this case, the details of spike generation are sacrificed for the sake of computational efficiency. As another example, if the details of dendritic interactions are significant to the question being asked in the model, then the use of an explicit multicompartmental model of individual cells and their dendritic regions is indicated (Koch, Poggio, and Torre 1982, 1983). If the nonlinearities of dendritic interaction are not of great significance to the particular response or network property of interest, then a simplified single-compartmental model of a cell might be sufficient (as in chapter 6). In other cases the type of physiological responses the simulation is expected to generate dictates the level of neuronal complexity. For example, in our model, data such as field potentials and current source density measurements require information about the spatial distribution of membrane currents in the simulated cortex to be calculated using a distributed model of the cell and its processes (see below).

9.2.2 Network Scale

At the network level a primary design consideration is one of scale. This is clearly seen in our model of piriform cortex where on the order of 10^3 cells represent a cortex that actually contains over 10^6 cells. Several basic approaches can be taken to deal with this problem. First, a modeler can reduce the scope of the model to include only a restricted portion of the actual structure. In this way a small region of the cortex can be simulated closer to its actual scale (see chapter 10). In this case the amount of cortical area simulated is restricted, but single-cell activity and local interactions are more accurately represented. Obviously, this approach is useful only if the primary aspects of the circuitry involved in the particular response being studied are preserved in this localized model, i.e., there are few relevant longer-range interactions. The second approach involves using sparse samples of single cells over a broad cortical area. This reduces the spatial resolution of simulated activity but allows the study of cortical phenomena that require nonlocal interactions. However, using cells as subsamples of a larger cortical area introduces the problem of compensation for the activity of cells not included in the simulation. This problem can be approached in several ways. For example, single modeled cells can represent the average response of a group of cells. The output of modeled "cells" in this case would consist of a continuous estimate of spatially averaged activity over a region of the actual network. This is roughly equivalent to using a rate-encoded output as is commonly done in more abstracted network simulations (Hopfield 1984; Hinton, McClelland, and Rumelhart 1986). An alternate representation preserves the single-spike nature of actual single-cell output. In this case the properties of single modeled cells are designed to resemble actual single cells as closely as possible, but synaptic strengths are adjusted to compensate for missing neurons. This is the approach that we have taken with our simulations as described in more detail below. The use of the single-spike output representation versus the spatial-average representation can be somewhat quantified. Appendix 9.D describes a measure based on an estimate of the connection probability between cells within different regions. In this case, the criterion used to select one representation over another is the preservation of the average or expected one-to-one connection characteristics between simulated cells. A detailed discussion of this issue with sample calculations related to the piriform cortex model can be found in Appendix 9.D.

9.3 Piriform Cortex and Model Structure

In the remainder of this chapter we will elaborate on the general issues outlined above by describing in detail the techniques that we have employed in carrying out structural simulations of olfactory cortex. However, because this is a structural model it will first be necessary to place the model in context by giving a general background description of piriform cortex. A more detailed description of this cortex can be found in Shepherd (1979) or Haberly (1985). The reader should also note that the intention of this chapter is to describe how the cortex is simulated and not to discuss the simulation results or conclusions themselves.

9.3.1 General Cortical Features

Piriform (olfactory) cortex is the primary olfactory cerebral cortical structure in all mammals. This structure is the focus of our modeling efforts because of its well-defined organization, the availability of physiological data, and its presumed capacity for memory and associative functions (Haberly 1985). The afferent sensory input to the piriform cortex is from the olfactory bulb, which itself receives direct projections from olfactory receptors. This cerebral cortical area is, therefore, unusually close to the sensory periphery, being just one structure removed. Bulbar input to the cortex is delivered via a fiber bundle known as the lateral olfactory tract (LOT). This fiber tract appears to make dis-

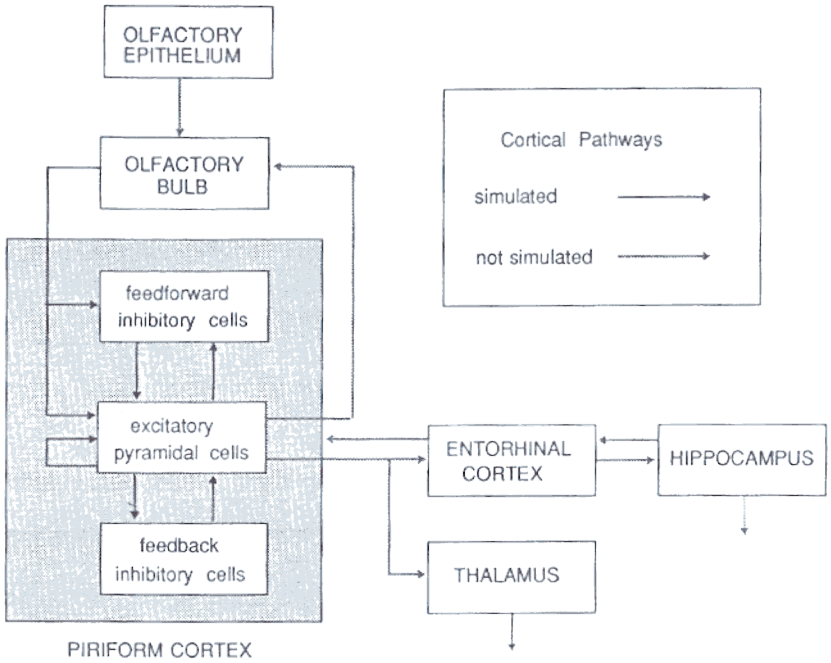

Figure 9.1
Block diagram of the olfactory system showing the basic connections between several primary structures. Arrows show the flow of information between these structures. The principal pathway in olfactory processing begins in the olfactory receptors, which project to the olfactory bulb. The olfactory bulb has extensive projections to other olfactory structures including the piriform or olfactory cortex. The piriform cortex has feedback projections to the olfactory bulb, intracortical association projections, as well as projections to the limbic system via entorhinal cortex.

tributed, nontopographic, excitatory connections with cortical neurons across the extent of the cortex (figs. 9.2, 9.3). This input arrives along the edge of the cortex and projects across its surface in a lateral fashion to a superficial layer (Devor 1976).

In addition to the afferent input connections from the olfactory bulb, there is also an extensive set of connections among neurons intrinsic to the cortex (figs. 9.2, 9.3). For example, the so-called association fiber system arising from the principal cortical cells, the pyramidal cells, makes sparse, distributed excitatory connections with other pyramidal cells across the cortex. There are also intrinsic inhibitory feedforward and feedback connections within the cortex mediated by two types of inhibitory interneurons with different properties. Pyramidal cell axons constitute the primary output of the piriform cortex and project to limbic structures such as entorhinal cortex (Haberly and Price 1978; Luskin and Price 1983a,b) whose neurons, in turn, project to the hippocampus. As such, piriform cortex has close ties to both the sensory periphery and to deeply buried forebrain structures of considerable current interest in neurobiology due to their postulated roles in learning and memory (Tanabe, Iino, and Takagi 1975; Devor 1977; Eichenbaum, Shedlack, and Eckmann 1980).

9.3.2 Neuronal Types

Pyramidal cells are the principal cell type in piriform cortex, and are believed to be exclusively excitatory (Haberly and Price 1978; Haberly and Bower 1984). There are also several populations of nonpyramidal cells or interneurons that can be distinguished on anatomical grounds (Haberly 1983; Haberly and Feig 1983). These neurons appear to be GABAergic and seem to mediate both feedback and feedforward inhibitory effects (see below). Our model is based on a single population of pyramidal cells plus two populations of inhibitory interneurons responsible for feedforward and feedback inhibitory influences (fig. 9.2). The model represents neurons across the full extent of the actual cortex (approximately 10 mm x 6 mm). In the simulation described here, we have modeled 1,500 cells of each type (50 cells x 30 cells) for a total of 4,500 cortical cells (fig. 9.3). The model also includes 100 cells representing the input to the cortex from the olfactory bulb.

9.3.3 Cortical Lamination

Piriform cortex, like all of the cerebral cortex, is a laminar structure that can be subdivided into layers based upon the segregation of different inputs and cell types. Piriform cortex, however, is composed of three

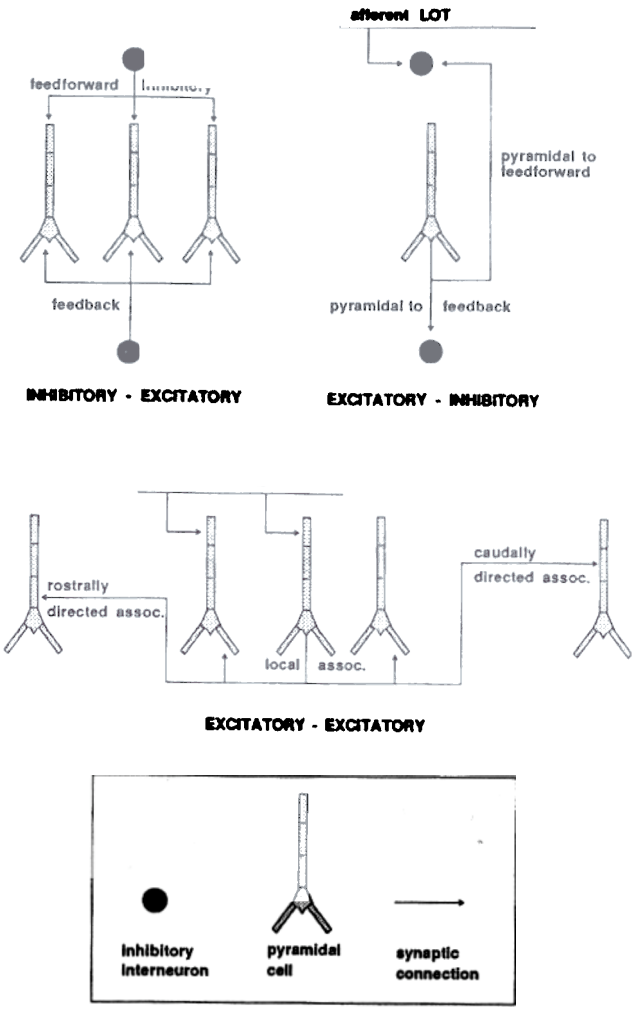

Figure 9.2
Basic interconnection patterns of cells within the model of piriform cortex as described in the text.

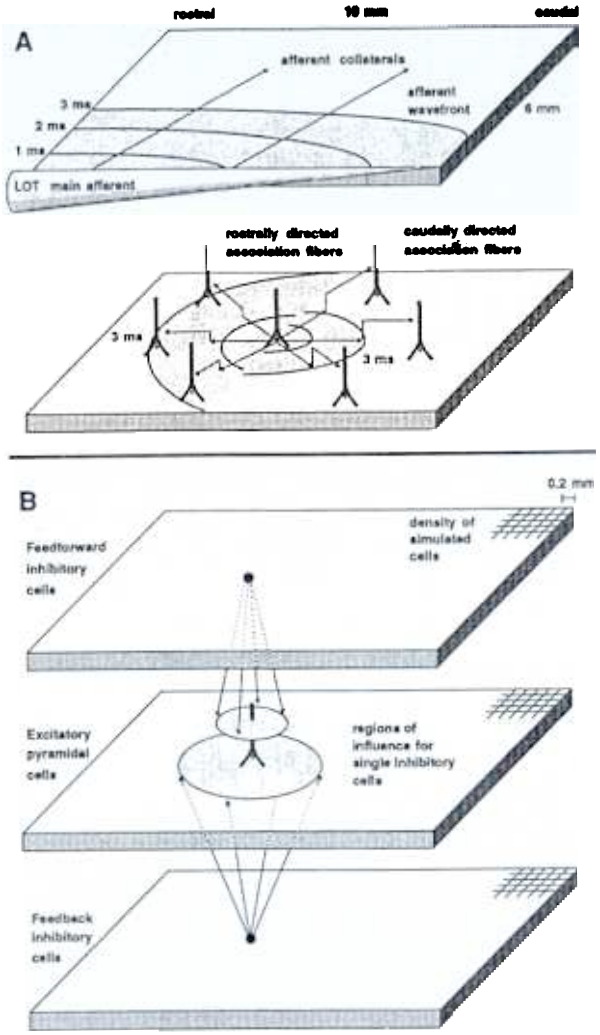

Figure 9.3
(A) The upper diagram shows characteristics of the afferent input to the cortex. The main lateral olfactory input tract (LOT) is seen at the lower edge of the diagram with bulbar input arriving from the left. The spread of activation following LOT stimulation is indicated by contours showing the location of the afferent wavefront at three successive times. The lower diagram shows the pattern of association fiber interconnection between a single pyramidal cell and pyramidal cells located rostral and caudal to it. The spread of activation is seen to be slower in the caudal than the rostral direction due to the difference in propagation velocities of the two types of association fibers. (B) A three-dimensional schematic diagram of the the three major cell types included in the model of piriform cortex—feedforward inhibitory interneurons, pyramidal cells, and inhibitory feedback interneurons. The grid in the upper right shows the scale of the model consisting of 1500 cells (50x30) of each type. Each grid site corresponds to the location of a modeled cell. The shaded regions indicate the regions of influence of the two types of inhibitory interneurons on pyramidal cells.

principal layers as compared with the six layers of neocortical structures. The most superficial layer (layer I) contains afferent axons that originate from mitral cells in the olfactory bulb as well as association axons arising from other pyramidal cells within the piriform cortex. Both fiber systems terminate on apical dendrites of pyramidal cells that extend through this layer. Based on these terminations, layer I can be further subdivided into the surface region where afferent fibers terminate (layer Ia) and the deeper regions containing terminations of the association fibers (layer Ib). There is evidence that layer Ib is further subdivided into a superficial region containing the terminations of caudally directed association fibers and a deeper region containing rostrally directed association fiber terminations (Haberly and Price 1977; Haberly and Bower 1984). Below layer I, the deeper layer II consists of densely packed cell bodies of both pyramidal cells and interneurons. Layer III contains basal dendrites of layer II pyramidal cells as well as cell bodies of deep pyramidal cells and other interneurons (fig. 9.3). Local connections between pyramidal cells terminate on basal dendrites in layer III. In the current model, only layer II pyramidal cells are simulated. The laminar pattern described serves as the basis of the compartmental model of the pyramidal cell in which distinct compartments correspond to laminar regions receiving particular types of input (see figs. 9.4, 9.5, 9.6, and Appendix 9.A).

9.3.4 Network Connections

Afferent Sensory Pathways As mentioned above, primary afferent input enters piriform cortex via the lateral olfactory tract projection from mitral cells of the olfactory bulb (fig. 9.3). Present evidence suggests that this projection is exclusively excitatory (Biedenbach and Stevens 1969a,b; Haberly 1973a; Haberly and Bower 1984) and extremely diffuse or nontopographic. These afferent fibers make excitatory synaptic connections with pyramidal cells and feedforward interneurons in layer Ia (Haberly 1985). This afferent input to the cortex is modeled as a set of independent fibers that make sparse connections with pyramidal cells and inhibitory interneurons. The actual degree of interconnection is varied according to the experimental paradigm being simulated. For example in some simulations we seek to reproduce physiological data obtained with shock stimulation of the afferent input system. Under these conditions of massive, synchronous afferent activation, the input to the cortex is represented as a bundle of afferent fibers that make excitatory synaptic connections with all pyramidal cells and feedforward interneurons in the cortex (Appendix 9.D). In other simulations where the intention is to replicate patterns of activity seen with more natural stimuli, we treat the afferent inputs independently and connect them more sparsely (Wilson and Bower 1988).

In both the actual cortex and the model, conduction velocities along axons are finite and vary with the axonal type (Haberly 1978). Signals travel along the main input tract from rostral to caudal, and are distributed across the cortex via many small collaterals (Devor 1976). In the model, signals proceed along the main fiber tract towards caudal cortex at a speed of 7.0 m/s. Collaterals leave the main fiber tract at a 45° angle and travel across the cortex at a speed of 1.6 m/s (Haberly 1973b).

In the actual cortex there is a diminution of afferent input to pyramidal cells moving from rostral to caudal that is reflected anatomically in the number of synaptic terminals (Price 1973; Schwob and Price 1978), and physiologically in the amplitude of shock-evoked potentials mediated by the afferent system (Haberly 1973b). To simulate this effect in the model, the strength of synaptic input due to afferent signals is exponentially attenuated with increased distance from the rostral site of stimulation (see w_{static} in eq. 9.5).

Association Circuitry In addition to the input connections from the olfactory bulb, there is also an extensive set of connections between the neurons intrinsic to the cortex (figs. 9.2, 9.3, 9.4). A principal component in these connections is the association fiber system that arises from pyramidal cells and makes sparse, distributed excitatory connections with other pyramidal cells all across the cortex (Biedenbach and Stevens 1969; Haberly and Bower 1984; Bower and Haberly 1986). The fibers appear to spread out radially from the originating cell and travel rostrally at a speed of 1.0 m/s, and caudally at a speed of 0.5 m/s (Haberly 1973b; Haberly 1978) making local connections on basal dendrites of other pyramidal cells and distant connections on apical dendrites. In the model, fibers originating from pyramidal cells follow the same pattern of interconnectivity and signals are propagated along each fiber with the corresponding delays (eq. 9.2). In the model, as a consequence of simulation scaling considerations (see section 9.2.2 and Appendix 9.D), association fiber interconnectivity is greatly increased as compared to that of the actual cortex.

The effect of monosynaptic association fiber input to a simulated cell is strictly excitatory. In the model, there is an attenuation over distance of the strength of synaptic input to other pyramidal cells reflecting a presumed decrease in a particular cell's influence with distance. The attenuation is consistent with the fall off in numbers of axon terminals

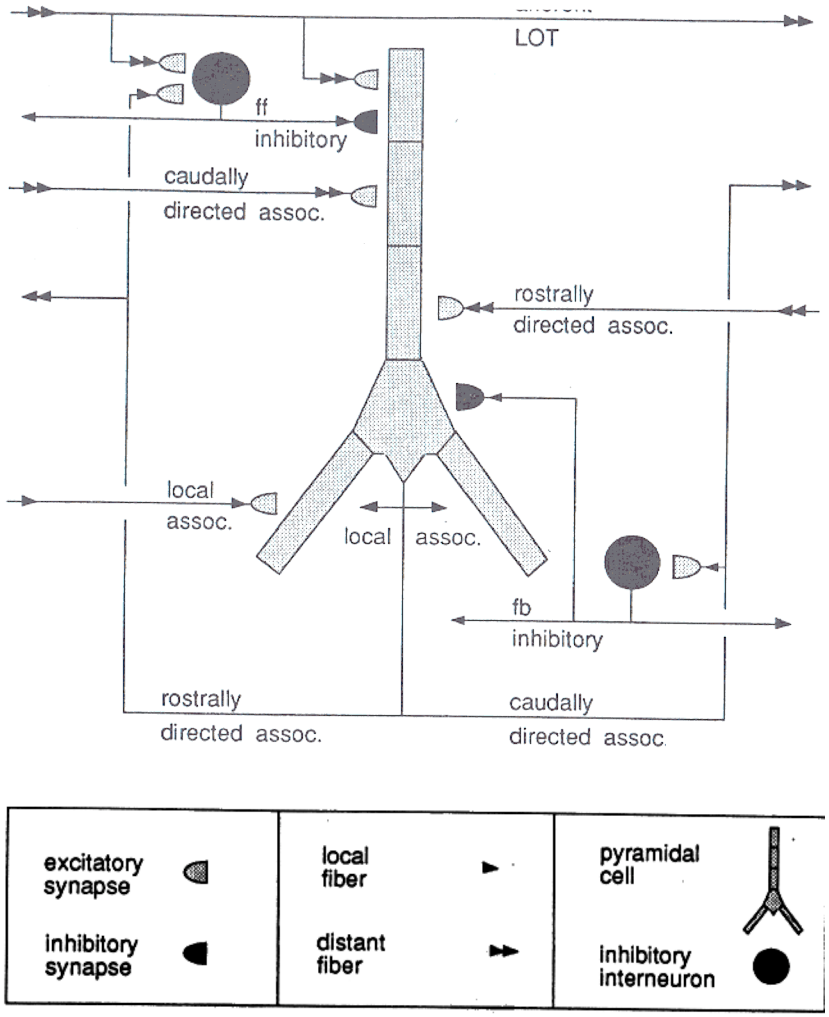

Figure 9.4
Simplified diagram of the local circuitry contained in the model of piriform cortex. The cell in the center represents a pyramidal cell, which is the primary excitatory cell type in the piriform cortex. Two other inhibitory cell types are shown as darkened circles adjacent to the pyramidal cell. The small semi-ellipses that appear next to the pyramidal and inhibitory cells indicate the location of synaptic connections. Darkened connections are inhibitory while lightened connections are excitatory. Arrows indicate the direction of propagation of signals originating from the various cell types, as well as the distance these fibers travel.

in local axon collaterals at greater distances from the originating neuron (Haberly and Bower 1982; Haberly and Presto 1986) and is modeled with an exponential function (see eq. 9.7). Rostrally and caudally directed association fibers have unique spatial attenuation constants. The level of attenuation asymptotically approaches a minimum value for each direction, consistent with physiological studies of association fiber systems in deafferented piriform cortex (L. Haberly, unpublished). In the model, the local region of excitation surrounding the cell, which terminates on the basal dendrites of its neighbors, has a radius of 2 *mm*. This value is an approximation since the actual value is not precisely known. Beyond this radius, connections are made onto apical dendrites. In the model, a pyramidal cell has no excitatory connection to itself (autapse), consistent with anatomical data (Haberly and Presto 1986).

Inhibitory Circuitry There is good evidence for two types of inhibition in piriform cortex, both of which are incorporated into the model. A well-documented Cl^- mediated feedback inhibition is thought to be generated by local interneurons that receive input primarily from local pyramidal cell association fibers as well as some afferent fibers (Biedenbach and Stevens 1969a,b; Haberly 1973a; Satou, Mori, Tazawa, and Takagi 1982; Haberly and Bower 1984; Tseng and Haberly 1986). The outputs of these inhibitory interneurons feed back to nearby pyramidal cells where significant conductance increases suggest a current shunting inhibitory mechanism (Scholfield 1978; Satou et al. 1982; Haberly and Bower 1984; Tseng and Haberly 1986). In the model these interneurons make inhibitory connections with the group of nearby pyramidal cells that lie within a 2 *mm* radius (again an estimate) where they activate a significant conductance increase to Cl^- at the level of the cell body (see below).

In addition to this shunting type inhibition, in the actual cortex a K^+ mediated inhibition appears to be generated by local inhibitory interneurons receiving primarily direct afferent input from the LOT as well as some associational input from pyramidal cells (Satou et al. 1982; Tseng and Haberly 1986). The outputs of these interneurons generate a long-latency, long-duration hyperpolarizing inhibitory potential in nearby pyramidal cells. Available evidence (Galvan, Grafe, and Bruggencate 1982; Satou et al. 1982; Tseng and Haberly 1986) suggests that this potential has a modest associated conductance increase and therefore may exert its inhibitory effect primarily via membrane hyperpolarization. In the model this hyperpolarizing inhibition is activated on the apical den-

drites of pyramidal cells by inhibitory neurons with both feedforward and feedback input.

9.3.5 Membrane Properties of Neurons and Synaptic Inputs

Channel Types In the model each population of neurons consists of single cells whose modeled membranes include synaptically activated ionic channels obeying simple channel kinetics and having a membrane capacitance and resistance (figs. 9.5, 9.6). The parameters that describe these properties have all been adjusted to replicate the temporal characteristics of transmembrane potentials found with intracellular recording using both *in vivo* (Haberly and Bower 1984) and *in vitro* (Haberly and Bower 1984) experimental preparations.

The membranes of modeled neurons include three types of ionic channels (table 9.1). The first type of channel is a modest-conductance sodium ion channel ($G_{peak} = 50\ nS$). This channel is activated by excitatory afferent and association fiber synapses, with an equilibrium potential of 100 mV above the average firing threshold of the cell ($E_{Na} = 55\ mV$). In this channel the time to onset of the conductance change following the arrival of a presynaptic action potential is 800 μsec, or a single synaptic delay. The duration of the change is 10 $msec$.

The second type of synaptically activated channel is a high-conductance, Cl^- mediated type. This channel is activated by inhibitory synapses from feedback interneurons and exerts a powerful current-shunting effect ($G_{peak} = 200\ nS$) on the membrane that drives it to a potential 20 mV below the average firing threshold ($E_{Cl} = -65\ mV$). In this channel the time to onset of the conductance change following the arrival of a presynaptic action potential is again a single synaptic delay. The duration of the change is 20–60 $msec$.

The third type of synaptically activated channel is a modest-conductance ($G_{peak} = 5\ nS$), K^+ mediated type. This channel is activated by the inhibitory synapses of feedforward interneurons, with an equilibrium potential 45 mV below the average firing threshold ($E_K = -90\ mV$). The time course of the conductance change induced in this channel is characterized by a long latency to activation following the arrival of a presynaptic action potential (30–50 $msec$) and a long duration (100–600 $msec$).

Cellular Structure The two types of inhibitory neurons are each modeled as single compartments, while two models of the excitatory pyramidal cells are used alternately during simulations. A simplified single-compartment pyramidal cell model (fig. 9.5) is used during large-

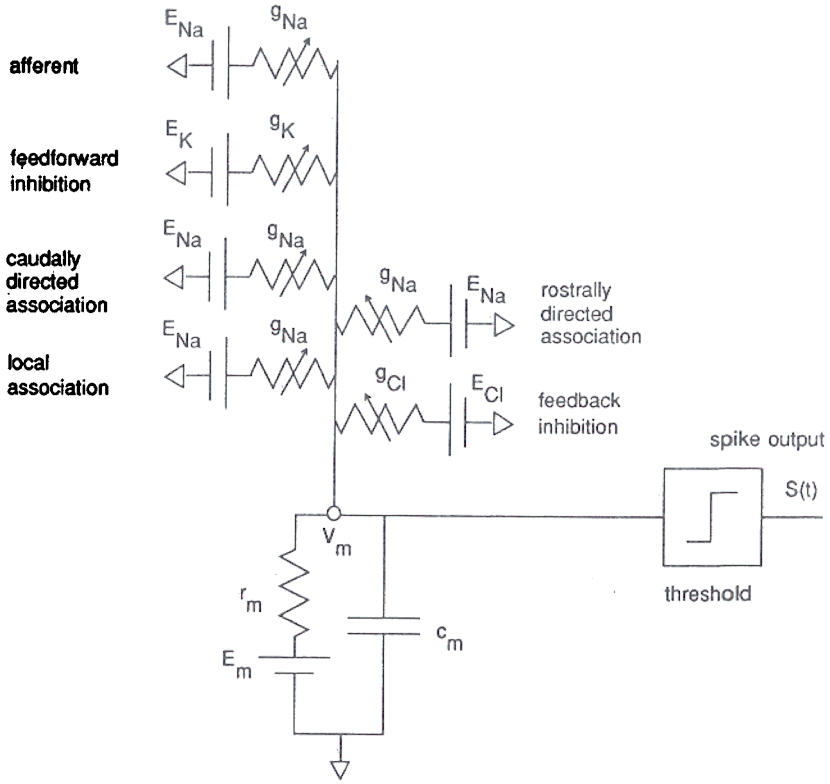

Figure 9.5
The circuit representation of a single-compartment pyramidal cell used in the model. Synaptic inputs arrive at channels containing a variable conductance g, and an ionic equilibrium potential E. The cell body is represented by a membrane resistance and a membrane capacitance. Spike events are generated when the potential across the membrane exceeds the threshold of the cell. These spike events are then propagated to other cells along delay line axons.

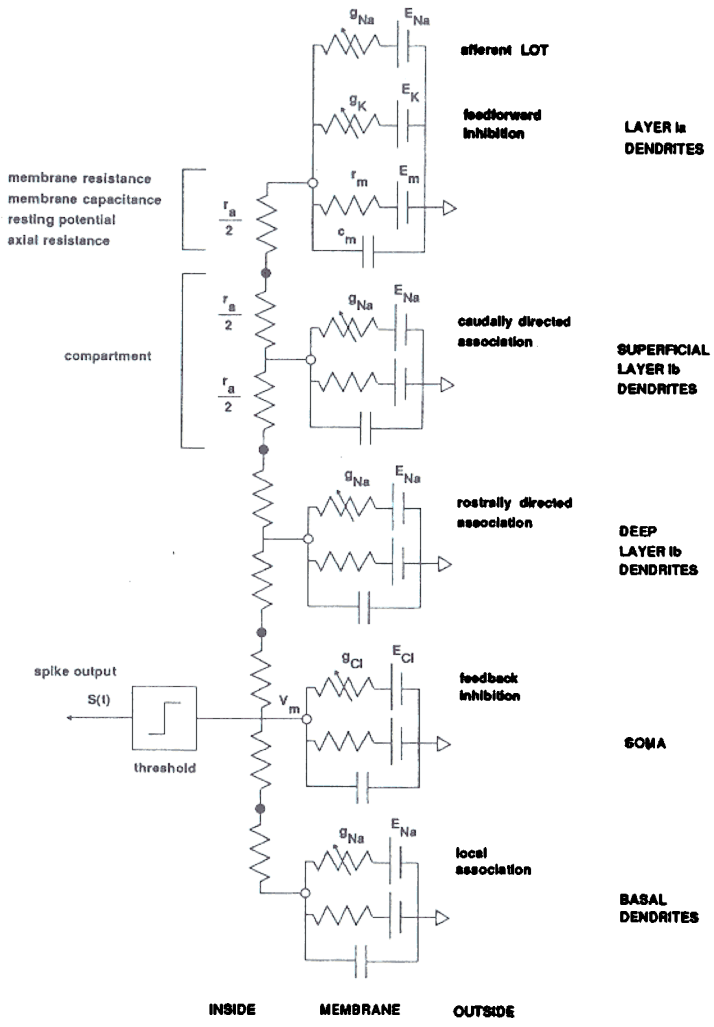

Figure 9.6
The circuit representation of a multicompartmental pyramidal cell used in the model. There are five compartments, each containing a membrane resistance, membrane capacitance, and resting potential, as well as one or more synaptically activated conductances.

scale simulations to establish the macroscopic cortical behavior. A more detailed five-compartment model (fig. 9.6) is then used to generate the spatial distributions of current flow within a single neuron using patterns of inputs generated by the large-scale model. These current distributions are needed for the calculation of extracellular field potentials (see Appendix 9.B).

As discussed in general above, this approach reflects a compromise between the number versus complexity of the neuronal elements simulated. In using the single-compartment model during network simulations it is assumed that the spatial interactions of current flow within the dendritic tree of the neurons are not significant to the responses being modeled. While this assumption must be made with caution, comparison of somatic membrane potentials generated by both the single- and multicompartmental approaches show good agreement with real experiments. Therefore, this simplification may be appropriate as an initial approximation, in order to study basic cortical phenomena. However, synaptic events occurring in the dendritic tree can impose significant nonlinearities on the integration of currents at the somatic level (Koch et al. 1983). Network simulations that include explicit dendritic structure will allow more detailed study of the effects of patterned dendritic activation on cellular activity. This is particularly important in exploring the more complex questions concerning computation within the network.

9.4 Specific Network Implementation

We will now consider the mathematical details of the implementation of the model of piriform cortex. While the network being considered represents a specific region of cerebral cortex, the general mathematical formulation is actually quite generic. In fact, it has served as the basis for the development of a general-purpose network simulation software package, which is capable of simulating a wide range of cortical as well as noncortical network structures. This software is described briefly in the last section of this chapter. This simulation has also served as a model for studying the general question of how neural network simulations can be implemented on parallel computers as discussed in chapter 12.

9.4.1 Neuronal Output and Transmission Delays

The output of each modeled cell i consists of an all-or-none action potential S_i with unit amplitude that is generated when the membrane potential V_i of the cell crosses a threshold T_i and the cell has not fired

should be δ function in continuous case

for a refractory period t_r. The thresholds for each cell have a normal distribution with a mean of $-45\ mV$ and a variance of $5\ mV$. The resting membrane potentials are set uniformly at $-70\ mV$.

$$S_i(t) = \begin{cases} 1 & V_i(t) \geq T_i, \text{ and } S_i(\lambda) = 0 \quad \text{for} \lambda \in [t - t_r, t] \\ 0 & \text{otherwise} \end{cases} \tag{9.1}$$

This output S_i propagates along fiber q to neurons j with a delay $t_{p(ijq)}$. The propagation delay from cell i to cell j along fiber q is

$$t_{p(ijq)} = \frac{L_{ij}}{\nu_q} \tag{9.2}$$

where L_{ij} is the the radial distance from the originating neuron i to the target neuron j, and ν_q is the velocity along the fiber type q that connects them.

There is an additional latency term $t_{\epsilon(ijq)}$ that represents the delay incurred at the synaptic junction. This corresponds to the time lag between the arrival of the presynaptic event and the generation of a postsynaptic response, nominally 800 μsec. Therefore the total time delay between generation of an action potential in the source cell and the generation of a postsynaptic event in the destination cell is

$$t_{t(ijq)} = t_{p(ijq)} + t_{\epsilon(ijq)} \tag{9.3}$$

9.4.2 Channel Conductance

When an action potential arrives at a destination cell it triggers a conductance change in a particular ionic channel described by the characteristic function $G(t)$ (see Appendix 9.C for the forms of this function). As already discussed, each class of ionic channel has a distinct set of parameters governing the time course, amplitude, and waveform of the conductance function (table 9.1). Therefore, the net channel conductance due to a single synaptic input $\hat{g}(t)$ is a function of presynaptic activation described by the function $S(t)$, and postsynaptic activation described by $G(t)$.

Since the characteristic postsynaptic conductance waveform $G(t)$ can have a time course longer than that of the presynaptic action potential, the influence of the discrete action potential event must be extended over the equivalent postsynaptic period. This effect can be described as the convolution of presynaptic events $S(t)$ with the postsynaptic conductance waveform $G(t)$. The net conductance in channel k of cell j due to input from cell i along fiber q is

$$\hat{g}(t)_{ijkq} = \int_0^{t - t_{t(ijq)}} G_{jk}(\lambda) S_i(t - \lambda - t_{t(ijq)}) d\lambda \tag{9.4}$$

where $t_{t(ijq)}$ is the total delay time for presynaptic events $S_i(t)$ to reach cell j along fiber q. This function describes the synaptic transformation for spike activity across a single connection. The implementation of this synaptic transformation is discussed in Appendix 9.C and in section 9.7.3.

9.4.3 Synaptic Connections

In many simulations, especially those exploring possible learning mechanisms (Wilson and Bower 1988), it is important to be able to change the strengths of individual synaptic connections as a consequence of network activity. These synaptic strengths are specified by a weight term $\hat{w}_{ijq}$ in the basic synaptic transformation function, which describes the strength of connection between cell i and cell j along fiber q.

Physiological experiments in piriform cortex suggest that synaptic effects on postsynaptic cells vary in an activity-dependent manner both in the short term (Bower and Haberly 1985) and in the long term (Bower and Rao 1986). In the model the effects of variable synaptic efficacy are simulated using a synaptic weight term of the form

$$\hat{w}_{ijq}(t) = w_{ijq}^{static} w_{ijq}^{variable}(t) \tag{9.5}$$

where w^{static} does not vary during a simulation and corresponds to the static distribution of synaptic terminals, and $w^{variable}$ is, in general, a function of presynaptic activation S, postsynaptic state V, and time t. Since these weights modulate the amplitude of the postsynaptic conductance they must be non-negative.

The resulting conductance change induced by the activation of a single synapse is given by

$$\hat{g}(t)_{ijkq} = \int_0^{t - t_{t(ijq)}} G_{jk}(\lambda) S_i(t - \lambda - t_{t(ijq)}) \hat{w}_{ijq}(t) d\lambda \tag{9.6}$$

This results in the weight applied in a "postsynaptic" fashion with the peak amplitude of the conductance continually varying at each time step.

A slightly modified form results in a "presynaptic" weighting in which the peak amplitude of the conductance is set at the time of arrival of the presynaptic signal S and remains at that value for its duration.

$$\hat{g}_{ijkq}(t) = \int_0^{t - t_{t(ijq)}} G_{jk}(\lambda) S_i(t - \lambda - t_{t(ijq)}) \hat{w}_{ijq}(t - \lambda - t_{t(ijq)}) d\lambda \tag{9.7}$$

9.4.4 Single-Cell Integration

The total conductance change induced in channel k of cell j is calculated by summing over all synaptic inputs to that channel.

$$g_{jk}(t) = \sum_{i=1}^{n_{cells}} \sum_{q=1}^{n_{fibers}(i)} \hat{g}_{ijkq} \tag{9.8}$$

The membrane potential V for a single compartment (cell) j with n_c channels is computed by integrating

$$\frac{dV_j}{dt} = \frac{1}{c_m} \sum_{k=0}^{n_c} [E_k - V_j(t)] g_{jk}(t) + I_{inject} \tag{9.9}$$

where I_{inject} takes into account any explicit current injection into the compartment and E_k is the equilibrium potential for channel type k. (See Appendix 9.A for the multicompartmental formulation.)

9.5 Setting Model Parameters

The majority of parameters in the model, such as axonal conduction velocities, time delays, the general properties of neuronal integration, and the major intrinsic neuronal connections, are estimated from anatomical and physiological measurements made within the actual cortex as described above (table 9.1). The weight term associated with each synapse is one of the primary variables subject to adjustment in the model. Determining actual values for synaptic weights in a cortical network as complex as piriform is an extremely difficult task. However, given that these weights modify conductance amplitude, modifying weights affects both the amplitude and time constants of membrane potentials. Therefore, actual experimental measurements of these factors can serve to constrain the operational range of weights. The second significant model variable not strongly constrained by experimental data is the pattern of specific cell-to-cell connections. In this case, experimentalists may never know the full matrix of interconnectivity for large-scale neural networks like piriform cortex. In the model, we constrain connectivity based on general connectivity patterns seen using anatomical and physiological techniques. However, it is an implicit assumption in this work that specific replication of actual connection patterns will not be necessary to derive functional information from these models.

9.6 Generation of Physiological Responses

Overall, our modeling of piriform cortex has proceeded in two stages. Our first objective was to replicate known cortical responses to various stimulation conditions (figs. 9.7, 9.8; Wilson and Bower 1988). Once this was accomplished we then proceeded to explore the possible functional capacities of this model (Wilson and Bower 1988). In both stages, to allow evaluation of simulated results, two neuronal output forms are generated by the simulation. First, time-varying values of membrane potential in modeled neurons are generated and directly compared with *in vivo* and *in vitro* intracellular recordings (fig. 9.7). Note again that the actual spike waveforms were not explicitly calculated but were "pasted" onto the actual membrane potential at the times corresponding to simulated spike output. Second, the simulations generate extracellular field potentials taken at discrete locations within the simulated cortex (fig. 9.7). This data is important for piriform cortex because of the wealth of field potential results available in both anesthetized and unanesthetized behaving animals (Freeman 1968, 1979a,b; Gault 1963, 1965). Field potential responses (evoked potentials, EEGs) are calculated by using a compartmental model of a pyramidal cell to establish the depth distribution of membrane currents given the pattern of input conductance changes generated by network simulation (see fig. 9.8 and Appendix 9.B). As mentioned above, further discussion of these results is beyond the scope of this chapter. The model has also allowed us to look at the spatial distribution of network activity (fig. 9.8).

9.7 Technical Implementation Issues

While the above discussion details the mathematical structure of the piriform cortex model, the computer simulation of this type of model raises specific technical implementation . In this section we will address several of these.

9.7.1 Integration Technique

Simulation of these models requires the numerical solution of systems of differential equations that describe the state of neurons as a function of time and space. These numerical techniques describe how one advances the state variables of the simulation (e.g., membrane potential) from time i to time $i+1$ through integration of the differential equations that describe the system. As discussed in Chapter 13, the primary factors

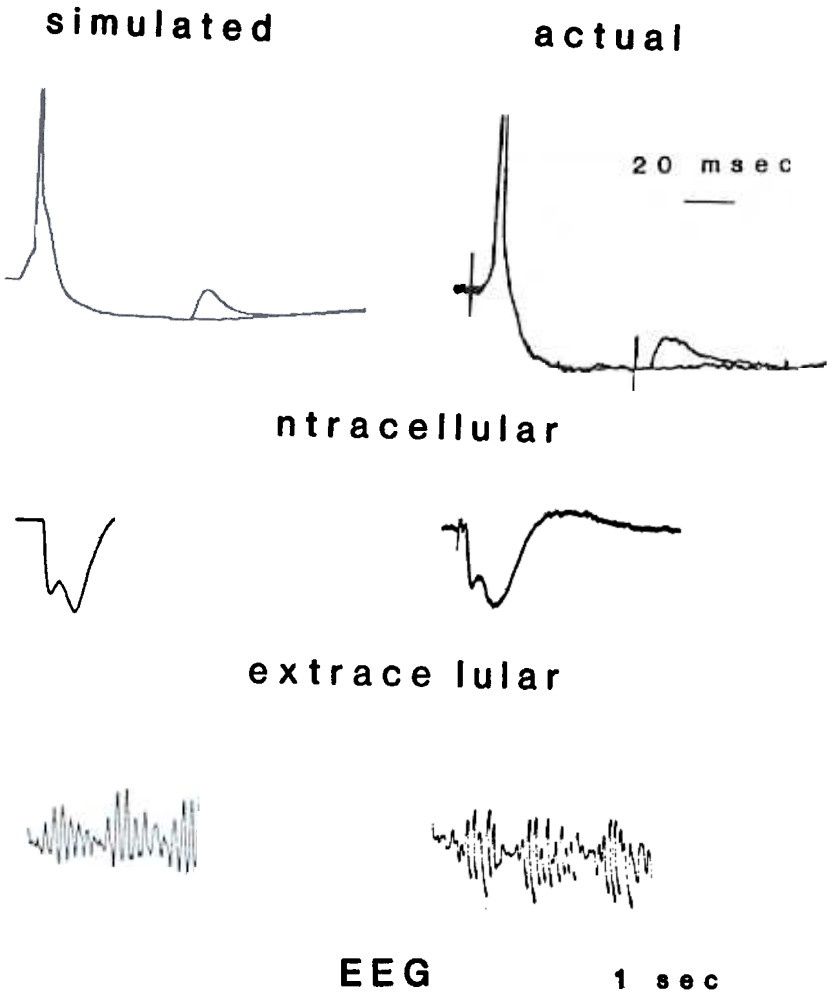

Figure 9.7
Upper right: Actual intracellular response recorded *invitro* (Bower and Haberly 1985) in response to paired shock stimuli applied to the LOT. The membrane potential of the cell was artificially depolarized to enhance the inhibitory hyperpolarization. Upper left: Simulated response under similar conditions. Middle right: Actual evoked potential response recorded *invivo* (Haberly and Bower 1984) in response to a single shock of the afferent LOT. Middle left: The simulated evoked potential contains the basic components of the actual data. Lower right: Actual EEG recorded from piriform cortex (Freeman 1960) consisting of a fast oscillatory component (30–80 Hz) modulated by a slower (3–8 Hz) component. Lower left: Simulated EEG with fast oscillations produced by alternating activation of excitatory and feedback inhibitory processes. The slow component coincides with the activation of the long-duration feedforward inhibitory process.

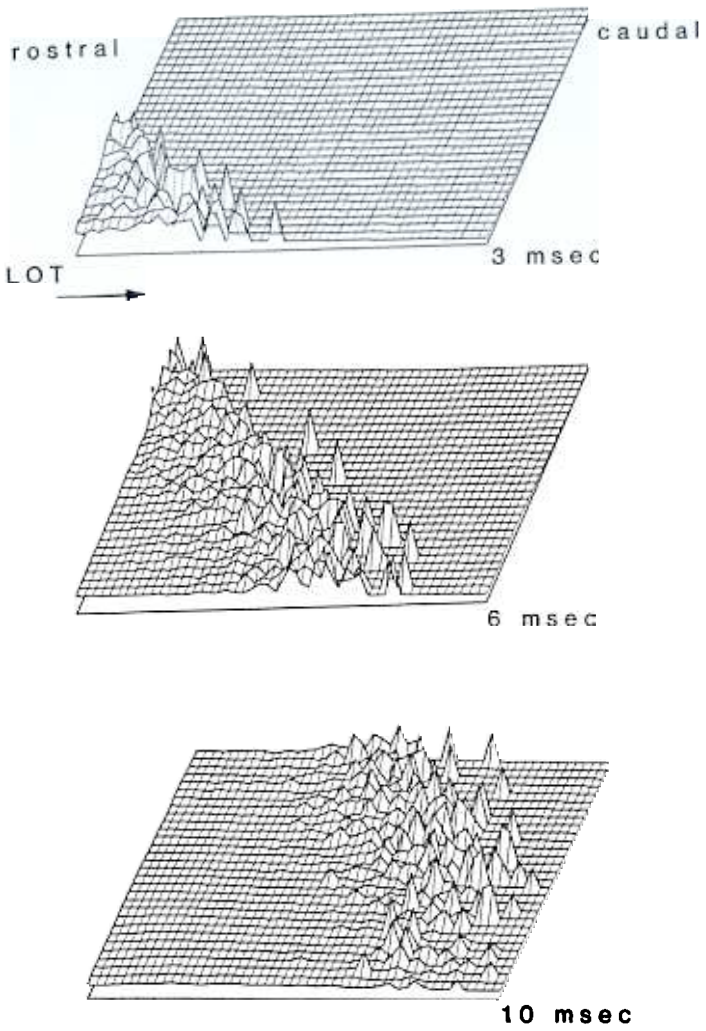

Figure 9.8
Three successive snapshots taken of the membrane potential of all simulated pyramidal cells following a shock stimulus applied to the afferent LOT. LOT input enters in the lower left corner of each frame. Activity is seen to propagate from rostral cortex to caudal cortex in a wave-like fashion. In frame 1 the activity is carried primarily along the fast, principal afferent fibers. By frame 3 the principal direction of the wavefront has changed as afferent input weakens and pyramidal cell spike activity begins propagating along the slower association fibers. (See fig. 9.3.)

that must be considered in selecting a particular technique are efficiency, accuracy, and stability. Efficiency refers to the amount of computation required to perform the integration. Accuracy reflects the degree to which solutions obtained match actual solutions. Stability is the behavior of the solution as time progresses. A system is convergently stable if it converges to a finite solution. However, methods that are stable are not necessarily accurate. Because the proper use of integration techniques is extremely important in these types of simulations, we have included a brief discussion of our results using several different techniques. For a thorough treatment of these methods refer to Chapter 13 as well as Press, Flannery, Teukolsky, and Vetterling (1986) or Smith (1985).

Large-scale networks can generally be treated as loosely coupled systems of ordinary differential equations that do not need to be solved simultaneously. In other words, evaluation of the state of any neuron in the system requires only past state information from other neurons and therefore can be solved independently for each neuron at every time step. These types of equations can typically be solved using simple numerical integration techniques. Two general categories of integration techniques will be discussed—explicit and implicit. In the following equations Δt refers to integration step size, y_i refers to the state variable at time i, and dy_i/dt is the time derivative of y evaluated at time i. For our purposes the state variable will typically be the membrane potential.

Explicit Techniques Explicit techniques solve for the state at discrete time $i+1$ using derivatives evaluated at or before i. They are referred to as explicit because the new state is based on the known history of the system. Explicit techniques include forward Euler and Adams/Bashforth multi-step.

Forward Euler

$$y_{i+1} = y_i + \Delta t \frac{dy_i}{dt} \tag{9.10}$$

Euler is the least accurate with marginal stability.

Adams-Bashforth: the following is the two-step Adams-Bashforth algorithm.

$$y_{i+1} = y_i + \frac{\Delta t}{2}\left(3\frac{dy_i}{dt} - \frac{dy_{i-1}}{dt}\right) \tag{9.11}$$

The Adams-Bashforth methods are more accurate but are also somewhat unstable.

Exponential: assuming a first-order form for the state equations with constant coefficients A and B over the interval Δt

$$\frac{dy}{dt} = -By + A \tag{9.12}$$

we can directly integrate the differential equation and obtain the solution. Through experimentation with our model, we have found that this technique has good stability and accuracy characteristics when used to solve membrane equations (MacGregor 1987).

$$y_{i+1} = y_i e^{-B\Delta t} + \frac{A}{B}(1 - e^{-B\Delta t}) \tag{9.13}$$

For example, given the membrane equation 9.9

$$\frac{dV}{dt} = \frac{1}{c_m}\Big[\sum_{k=0}^{n_{channels}} (E_k - V)G_k + I\Big]$$

$$A = \frac{1}{c_m}\sum E_k G_k + I \tag{9.15}$$

$$B = \frac{1}{c_m}\sum G_k \tag{9.16}$$

Implicit Techniques Another class of numerical integration schemes are the implicit techniques that solve for the state at time $i+1$ using the derivative evaluated at $i+1$. Common implicit techniques include Gear second-order and trapezoidal integration.

Gear

$$y_{i+1} = \frac{4}{3}y_i - \frac{1}{3}y_{i-1} + \frac{2}{3}\Delta t \frac{dy_{i+1}}{dt} \tag{9.17}$$

Trapezoidal:

$$y_{i+1} = y_i + \frac{\Delta t}{2}\left(\frac{dy_{i+1}}{dt} + \frac{dy_i}{dt}\right) \tag{9.18}$$

Comparison Overall, the explicit exponential and the implicit trapezoidal technique were found to be the best integration algorithms for solving neuronal membrane equations in terms of efficiency, stability, and accuracy.

9.7.2 Step Size

Several factors are involved in selecting the simulation step size Δt. One consideration is the maximum integration step size that can be used to update the neuronal state variables. This can be affected by the numerical algorithm used as well as the conditions being simulated. As a general rule the integration time step should be less than 1/5 of the fastest time constant of interest to minimize integration errors. In practice, lower-order integration techniques such as forward Euler require substantially smaller time steps.

The characteristics of the conductance waveform $G(t)$ will have a strong influence on the errors introduced during integration and therefore on the step size selected. Sudden or high amplitude conductance changes can result in rapid changes in the transmembrane current (eq. 9.9), which must be integrated with small step sizes to minimize errors. Another consideration in step size selection is the minimum propagation delay between elements. The step size chosen should not be made larger than this quantity if accurate intercell propagation timings are to be preserved. In general the maximum error in intercell propagation times will be equivalent to one-half the step size selected, and therefore the maximal timing error between events arriving at a cell from different sources will be equivalent to the step size. In cases where there is a large discrepancy between the step size dictated by integration and by intercell delay an approach involving multiple step sizes may be appropriate.

9.7.3 Implementation of the Synaptic Transformation

The transformation of neuronal output (spikes) to dendritic input (conductance) can be described as a convolution of the incoming spike signal with a characteristic conductance waveform. Two basic techniques can be used to perform this operation.

Explicit Convolution Two approaches can be taken to directly implement the convolution described in eq. 9.4. In both cases a history of spike signals $S(t)$ must be maintained for each cell. To reduce computation time, we restrict the interval over which incoming spikes are convolved with the channel conductance waveforms $G(t)$ to t_d. The

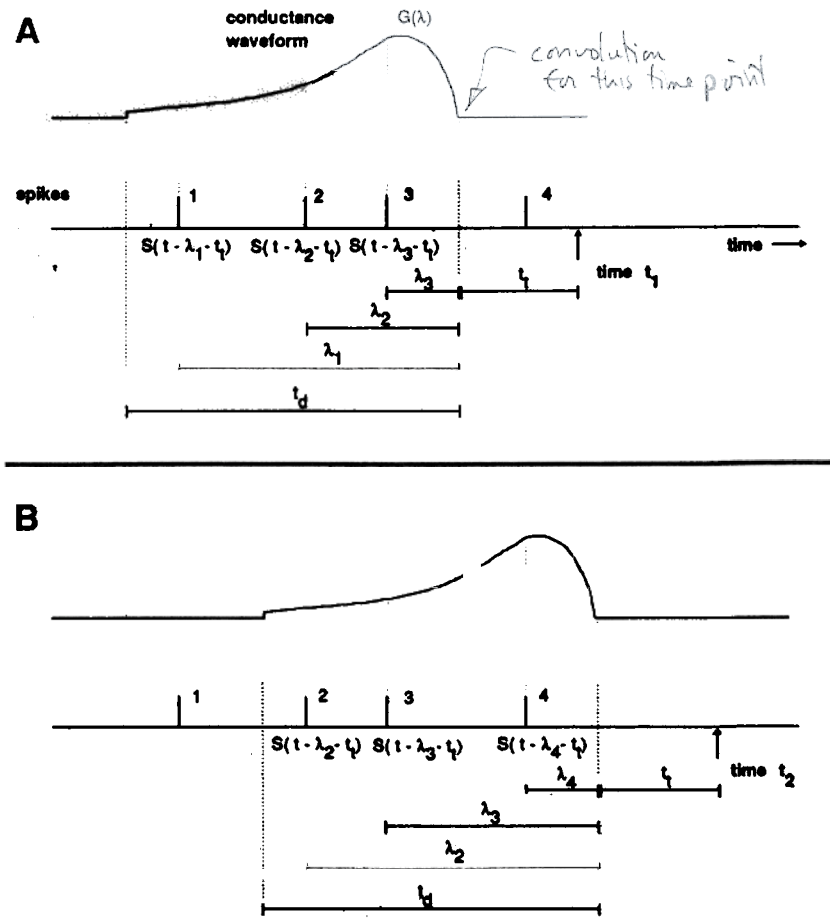

Figure 9.9
A schematic representation of the convolution operation used to transform spike output $S(t)$ into synaptic conductance change $\hat{g}(t)$ (eq. 9.4). (A) shows the spike history of a single cell being mapped onto a synaptic target at time t_1 using the conductance waveform $G(t)$. The total conductance change induced by the source cell is computed as $\hat{g}(t_1) = G(\lambda_1)S(t_1 - \lambda_1 - t_t) + G(\lambda_2 - t_t)S(t_1 - \lambda_2 - t_t) + G(\lambda_3 - t_t)S(t_1 - \lambda_3 - t_t)$. (B) shows the same mapping at a later time t_2. The time between the leading edge of the conductance waveform G and the current time t_2 remains constant (total delay t_t, eq. 9.3) while the spikes contained within the convolution interval t_d change. The total conductance change induced by the source cell at the new time t_2 is computed as $\hat{g}(t_2) = G(\lambda_2)S(t_2 - \lambda_2 - t_t) + G(\lambda_3 - t_t)S(t_2 - \lambda_3 - t_t) + G(\lambda_4 - t_t)S(t_2 - \lambda_4 - t_t)$.

length of time over which history must be maintained is given by $t_t + t_d$. The t_t factor is required to implement propagation delay. This results in a modified expression for the conductance

$$\hat{g}_{ijkq}(t) = \int_0^{t_{d(k)}} G_{jk}(\lambda) S_i(t - \lambda - t_{t(ijq)}) d\lambda \qquad (9.19)$$

Assuming that the conductance waveform function $G(t)$ is only a function of time, the convolution with the discrete signal $S(t)$ can be precalculated over the interval $[0,t_d]$ and stored at the destination site. Since the time spent communicating information between cells is a significant computational overhead, this approach can potentially reduce the amount of computation at the cost of storage proportional to $t_d/\Delta t$ per synaptic target.

An alternate approach involves evaluating eq. 9.17 at each point within the interval t_d in step with the simulation. This requires no additional storage but adds additional communication proportional to $t_d/\Delta t$ since the term $S(t)$ (the signal sent between neurons) must be accessed at each step.

Second-Order System A second approach uses a time differential representation of the conductance waveform. The conductance is modeled as a damped oscillator that has an impulse response of the form shown in eqs. 9.33 and 9.36. The impulse is provided by the spike input $S(t)$. In this case the value of the conductance is computed using current state information and explicit convolution is not necessary. This reduces the amount of history that must be maintained from $t_t + t_d$ to t_t. See Appendix 9.C for the implementation details.

Comparison The advantage of explicit convolution is that arbitrary conductance waveforms are easily implemented. The disadvantage is that there is either a storage or computational overhead that is on the order of the number of synaptic connections. The second-order or differential representation typically requires less computation and storage but implementation of arbitrary conductance functions is not straightforward. See Appendix 9.C for detailed comparisons.

9.7.4 Computational Requirements

The simulations of piriform cortex described were carried out on a Sun Microsystems 3/260 model microcomputer equipped with 32 *Mbytes* of memory and a floating point accelerator. These simulations of 4,500 cells (1,500 of each type) ran at a nominal rate of approximately 10 *cpu sec* per step. With a step size of 0.1 *msec* the average time for a 200 *msec* simulation was 300 *cpu min*. Using explicit convolution to compute the conductance, over 90% of the computation involved the distribution of information between elements, with the remaining time spent updating the states of individual elements. The overall computation time was very sensitive to fluctuations in activity level. Using the second-order representation, the computation was more evenly balanced between spike distribution (60%) and state update (40%) with less sensitivity to fluctuations in activity. The memory required for these simulations exceeded 24 *Mbytes* primarily due to storage of synaptic connections. This scale of simulation was operating at the upper limits of the computing resources available. As would be expected, simulations that are on the scale of hundreds of elements operate at a considerably faster rate and utilize more modest amounts of memory. For example, equivalent simulations using 300 cells (100 of each type) ran at a rate of 0.05 *cpu sec* per step. The average time for a 200 *msec* simulation was 1.5 *cpu min* and the memory required for this scale of simulation was approximately 2 *Mbytes*. Thus implementation of this type of simulation on the scale of hundreds of cells is quite feasible even on currently available PC class machines.

9.7.5 Storage Considerations

A problem in using individually specified synaptic weights and delays is that their number can expand as the square of the number of neurons in the simulation. This overhead in storage can limit the size of the network. An alternative representation for synaptic connections can be used if uniqueness of individual synapses is not critical. This representation takes the form of connection rules that describe how a representative cell connects with other cells using coordinates relative to the representative cell. The information stored in this source-relative connection scheme is both a delay and synaptic weight term. In this way a representative connection pattern takes up an amount of space proportional to that required by connections from a single cell.

9.8 The Simulator

Instructed by the model of piriform cortex just described, we have been developing a general-purpose simulation tool that allows the construction of arbitrary neuronal simulations. This effort was motivated by several factors. First, we believe that powerful but flexible simulation

software will increase the likelihood that neurobiologists will build structural models of their systems. Second, we hope that the availability of a standard for simulations of this type would provide a means for exchange of modeling data and results and therefore accelerate progress in understanding these exceedingly complex neuronal structures. Third, we believe that a critical issue for the acceptance of simulations as a tool in neurobiology is the degree to which simulation results can be replicated. The availability of standard simulation software makes this much easier to accomplish. Fourth, while any neural network simulation designed with a particular network in mind can be optimized for maximum efficiency, a tremendous time investment is required to build such a system. In the process of designing the simulator we have found that the principal features of most neuronal networks are common enough that a general network simulator is not only possible but also remarkably efficient.

9.8.1 Overall Simulator Structure—in Brief

Within the network simulator GENESIS, components are constructed out of basic building blocks called elements. In the most general sense, an element is a structure that receives inputs, performs transformations on these inputs, and generates outputs. Thus, an element can represent a membrane compartment, a simple cell, or a complex dendritic structure. This is the principal source of the simulator's generality. Once constructed, these components can then be combined into networks that have varied classes of interconnectivity, from graded signals sent with no delay, to discrete signals that propagate with finite velocity. Single elements maintain lists of input and output transformation modules. The simulator maintains a library of these modules that can be extended by the user. This extendible modularity allows multiple classes of transformations within an element. Since each element is a distinct functional unit, homogeneous structure within a network is also not a limitation. Elements are maintained in a hierarchical form allowing the simulation of models at various levels of complexity and detail. Figure 9.10 shows a block diagram of the simulator implementation of the model of piriform cortex.

The simulator shell environment allows interactive access to user-expandable network specification functions and allows interactive runtime specification and manipulation of model structures and parameters. The graphical specification and display tools provide the means to construct custom graphics interface environments for individual simulations.

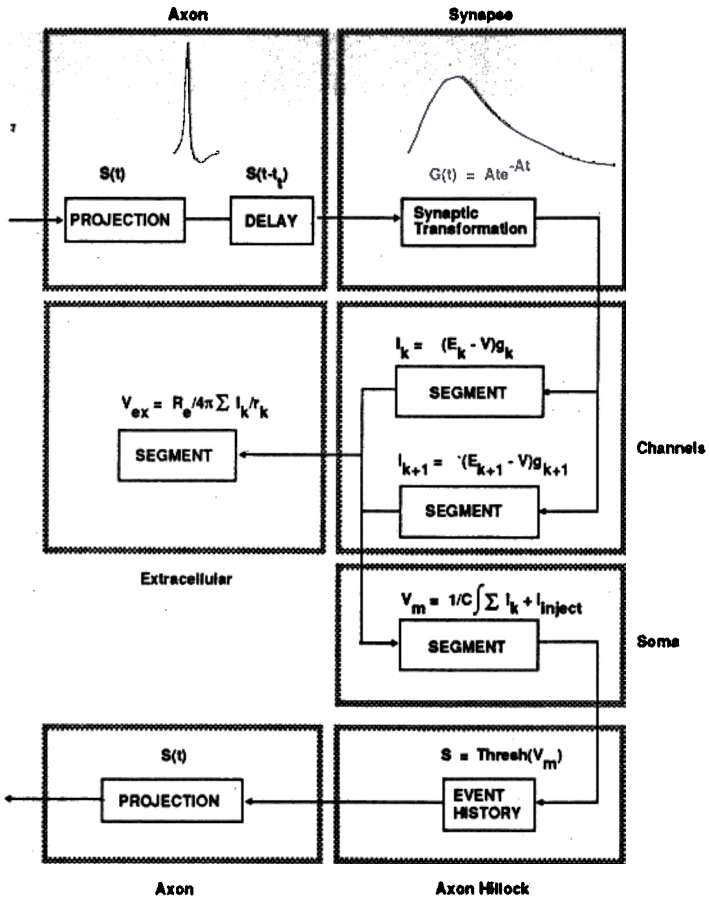

Figure 9.10
Schematic diagram showing the primary components of the single-cell model used in the simulations of piriform cortex and their mathematical correlates. The structure reflects the implementation of the model in the network simulator GENESIS.

9.8.2 Parallel Implementation

The object-oriented nature of the simulator design allows the basic simulator components to be easily broken up into functional pieces. The way in which these pieces can then be distributed across a parallel architecture is discussed in chapter 12. An important point is that since information is constrained to flow through simulator communication facilities, support for parallel architectures can be provided in a transparent, controlled fashion while still allowing the flexibility of user-defined functionality. The ability for the user to easily add varied functionality to the basic simulator framework is a critical factor in the simulator design.

9.8.3 Simulator Requirements

The simulator itself requires 300 *Kbytes* of memory. The optional graphics module adds an additional 300 *Kbytes*. A moderately complex cell requires from 500–1000 *bytes* with an additional 16 *bytes* for each connection. Thus, a small fully connected network on the scale of 100 cells uses approximately 200 *Kbytes*. The simulator runs under the Unix operating system. The graphical specification and display facilities have been written using the X windowing system for maximum portability. The simulator runs on a number Unix-based systems including SUN3, SUN4, SUN386i, and Masscomp computers. It is designed to be easily portable to other Unix-based systems.

The address of Matthew Wilson and James Bower is Division of Biology 216-76, California Institute of Technology, Pasadena, California 91125. Readers interested in further information on the simulator should send requests via electronic mail to genesis@aurel.caltech.edu .

Appendix 9.A: Multicompartmental Model

In the multicompartment implementation of the pyramidal cells, each compartment consists of one or more synaptic input channels, a membrane resistance r_m, and a membrane capacitance c_m (fig. 9.6).

$$r_m = \frac{R_m}{\pi l d} \tag{9.20}$$

$$c_m = C_m \pi l d \tag{9.21}$$

where l is the length of the dendritic segment, and d is its diameter. R_m is the membrane resistivity and C_m is the capacitance per unit area.

As in the case of single-compartment neurons, each channel k consists of a time-varying conductance $g_k(t)$ in series with a voltage source E_k representing the equilibrium potential of the ion associated with the channel. However, in this case, each compartment is also coupled to its adjacent compartment(s) with an axial resistance r_a. This axial resistance is divided in two and placed on either side of the lumped membrane representation for a symmetric compartment.

$$r_a = \frac{1}{2}\left[\frac{4R_a l}{\pi d^2}\right] \tag{9.22}$$

where R_a is the axial resistivity. Therefore, the input to each compartment has two primary components, an axial and a transmembrane current.

If we select a compartment and designate its two axial ends with + and − then the total axial current into the compartment is given by

$$I_a = I_a^- + I_a^+ \tag{9.23}$$

where the individual axial components from the two adjoining compartments are calculated by

$$I_a^- = \frac{V^- - V}{r_a^- + r_a} \quad , \quad I_a^+ = \frac{V^+ - V}{r_a^+ + r_a} \tag{9.24}$$

V is the membrane potential of the compartment. V^{+-} is the membrane potential of the compartment on the + and − side of the compartment respectively and r_a^{+-} is the axial resistance of that compartment. I_a^{+-} is the current entering the compartment from the +− side. To simplify notation the time-dependent variables $V(t)$ and $I(t)$ are written as V and I.

The boundary conditions assume sealed ends with $I_a^{+-} = 0$. This can be extended to a branching structure using

$$I_a^{+-} \sum_{j=1}^{N^{+-}} \frac{(V^{j+-} - V)}{r_a^{j+-}} \left[1 + r_a \sum_{j=1}^{N^{+-}} \frac{1}{r_a^{j+-}} \right. \tag{9.25}$$

where N^{+-} is the number of compartments adjoining the + and − side of the compartment respectively.[1] With $N^{+-} = 1$ this simplifies to eq. 9.20, which applies a dendritic cable.

The ohmic portion of the transmembrane current is given by

$$I_m = \frac{E_{rest} - V}{r_m} + \sum_{k=0}^{n_{channels}} (E_k - V) g_k(t) \tag{9.26}$$

The first term represents the passive leakage component with resting potential E_{rest} and leakage resistance r_m. The summation term gives the input through synaptically activated conductances $g_k(t)$. These conductances are activated by the arrival of presynaptic signals.

The membrane potential V of each compartment is calculated by integrating the current across the membrane capacitance. The differential change in membrane potential with time is given by

$$\frac{dV}{dt} = \frac{1}{c_m}(I_a + I_m) \tag{9.27}$$

Appendix 9.B: Field Potentials

Field potentials are generated when membrane currents generated by neurons pass through the extracellular space. These currents can be set up both by active output processes such as action potentials, as well as by input processes such as synaptic currents. The field potential at any point will be composed of the linear superposition of fields generated by current sources (current from the intracellular space to the extracellular space) and sinks (current from the extracellular space into the intracellular space) distributed along multiple cells. In the following discussion the term "current source" will be used to refer to both sources and sinks.

The value of the field potential depends on the extracellular resistivity, the location and amplitude of the current sources, and the location of the recording electrode relative to the current sources. For example, when the recording electrode is approximately equidistant from a large number of current sources it will measure the spatially averaged field produced by these sources. This corresponds to an electrode placed on the cortical surface measuring the fields generated by a sheet of neurons beneath it (as in the EEG). As a separate example, an electrode placed very close to a smaller number of current sources would preferentially record the fields generated by those sources. This corresponds to a microelectode placed close to the spike-generating mechanism of a single cell to measure its isolated spike output (as in extracellular single-unit recording).

[1] Note that this formulation is identical to that for asymmetric compartments with the addition of the right-hand denominator term. Thus the symmetric compartment requires slightly more computation than its asymmetric counterpart but is a more accurate representation of neurons consisting of smaller numbers of compartments.

The exact contributions to the field potential by neuronal activity depend largely on the geometry of single cells and network circuitry, as well as the spatial and temporal patterns of activity both within a cell (e.g., sequence of dendritic activation), and among groups of cells (e.g., synchrony of firing).

Consider the multicompartmental model used to generate the spatial distributions of membrane currents. The model computes a single transmembrane current I_m intended to represent the "lumped" current across a section of membrane. If we assign each compartment an x, y, z coordinate, we can treat each lumped transmembrane current I_m as a point current source located at those coordinates.

For point current sources distributed in a linear noncapacitive medium we have (Nunez 1981)

$$V_f(t) = \frac{R_e}{4\pi} \sum_{j=1}^{n_{cells}} \sum_{k=1}^{n_{compartments}} \frac{I_{m(jk)}(t)}{r_{jk}} \tag{9.28}$$

where

$$r_{jk} = \left[(x' - x_{jk})^2 + (y' - y_{jk})^2 + (z' - z_{jk})^2 \right]^{\frac{1}{2}} \tag{9.29}$$

The coordinates (x', y', z') give the location of the recording site. The coordinates (x^{jk}, y^{jk}, z^{jk}) give the coordinates of the compartment k in cell j. r_{jk} is the distance from compartment k in cell j to the recording site. $I_{m(jk)}$ is the transmembrane current in compartment k of cell j. R_e gives the extracellular resistivity per unit distance assuming a homogeneous extracellular medium (constant resistivity). V_f is an estimate of the extracellular field potential at (x', y', z').

Thus, in order to compute an estimate of the field potential the total transmembrane current for each compartment in each cell is summed according to the inverse distance of the current source (compartment) from the simulated recording site.

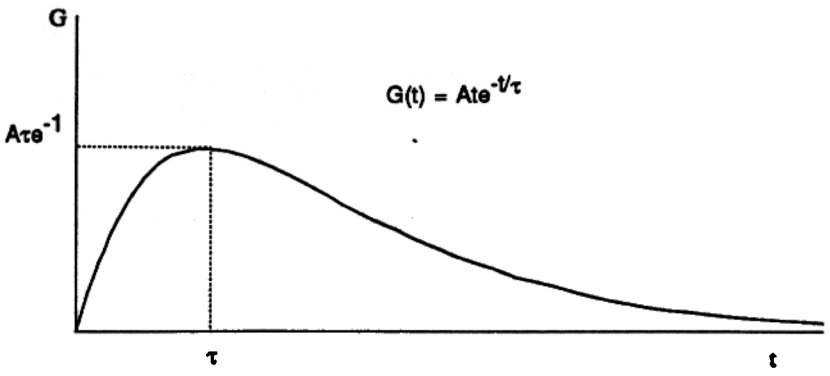

Figure 9.11
Waveform of the alpha function (eq. 9.33)

Appendix 9.C: Synaptic Transformation

Synaptic Convolution Operation

Truncating the conductance function $G(t)$ after time t_d as in eq. 9.19 can introduce rapid changes in transmembrane current. These fast transients can induce numerical instability in the integration of the membrane potential. Several methods can be used to avoid this problem. One technique is to extend the integration interval t_d such that it is many time constants τ in duration. This approach minimizes the discontinuities at the expense of increased computation. Another approach involves modifying the conductance function to eliminate discontinuities. One modification of the conductance function uses a quarter-period of a cosine function applied after the peak of $G(t)$ to force it smoothly to zero after the desired duration t_d. In this way the peak amplitude, peak latency, and rise time of the original conductance function $G(t)$ are preserved while discontinuities at time t_d are eliminated.

$$\hat{G}(t) = G(t)\left[(1 - U(t - t_{peak})) + U(t - t_{peak})cos\left[\frac{\pi}{2}\frac{(t - t_{peak})}{(t_d - t_{peak})}\right]\right] \quad (9.30)$$

where t_{peak} is the time to peak of the conductance function and $U(t)$ is the unit step function.

Second-order Synaptic Transformation

The general second-order form of the differential transformation equation is

$$\ddot{G} + \alpha\dot{G} + \beta G = x(t) \quad (9.31)$$

$$\alpha = \frac{\tau_1 + \tau_2}{\tau_1\tau_2}, \beta = \frac{1}{\tau_1\tau_2} \quad (9.32)$$

The impulse response of this system ($x(t) = \delta(t)$) with initial conditions of $G(0) = 0$ has two basic forms.

Alpha function Under the condition where $\tau_1 = \tau_2 = \tau$,

$$G(t) = te^{-t/\tau} \quad (9.33)$$

The time to peak of this form is

$$t_{peak} = \tau \quad (9.34)$$

and the peak value at that time is

$$G_{peak} = \tau e^{-1} \quad (9.35)$$

Dual exponential For $\tau_1 \neq \tau_2$,

$$G(t) = \frac{\tau_1\tau_2}{\tau_1 - \tau_2}(e^{-t/\tau_1} - e^{-t/\tau_2}) \quad (9.36)$$

The time to peak is given by

$$t_{peak} = \frac{\tau_1\tau_2}{\tau_1 - \tau_2}ln(\frac{\tau_1}{\tau_2}) \quad (9.37)$$

and the peak value at that time is

$$G_{peak} = \frac{\tau_1\tau_2}{\tau_1 - \tau_2}(e^{-t_{peak}/\tau_1} - e^{-t_{peak}/\tau_2}) \quad (9.38)$$

Practical implementation The objective is to solve the second-order equation for $G(t)$ at each time step t and then solve for the net conductance change $\hat{g}(t)$. The second-order system can be described by two first-order equations.

$$\dot{z} = \frac{-1}{\tau_1} z + x(t) \tag{9.39}$$

$$\dot{G} = \frac{-1}{\tau_2} G + z \tag{9.40}$$

In our case $x(t) = S(t - t_t)$. If "presynaptic" weighting is included this becomes $x(t) = S(t - t_t)w(t)$.

These equations can be numerically integrated to yield $G(t)$ using the techniques mentioned in section 9.7.1. The net conductance is then calculated by

$$\hat{g}(t) = \frac{g_{peak}}{G_{peak}} G(t) \tag{9.41}$$

or with "postsynaptic" weighting

$$\hat{g}(t) = \frac{g_{peak}}{G_{peak}} G(t)w(t) \tag{9.42}$$

where g_{peak} is the desired peak conductance value.

The following equations describe one method for advancing the solution to $G(t)$ from time t to time $t + \Delta t$. If spikes are considered to take the form of impulse functions then $x(t) = S(t - t_t)/\Delta t$, where $S(t - t_t)$ is the amplitude of a spike that occurred at time $t - t_t$. The variable z can then be evaluated as

$$z_{t+\Delta t} = z_t e^{\Delta t/\tau_1} + \frac{S(t - t_t)}{\Delta t} \tau_1 (1 - e^{\Delta t/\tau_1}) \tag{9.43}$$

and the conductance G is given by

$$G_{t+\Delta t} = G_t e^{\Delta t/\tau_2} + z_t \tau_2 (1 - e^{\Delta t/\tau_2}) \tag{9.44}$$

The net conductance is then obtained as in eqs. 9.41 or 9.42.

Comparisons

We can compare the computational overhead associated with various implementations of the synaptic transformation by calculating estimated simulation time.

N_{sp} = the number of spikes in the interval t (total simulation time)
N_{syn} = number of synaptic connections
N_{st} = number of time steps in the interval t_d (convolution interval)

N_t = number of time steps in the interval t
N_{ch} = number of channels or synaptic targets
T_c = computation per step for communication (spike propagation)
T_s = computation per step for second-order conductance calculation
T_g = computation per step for convolution conductance calculation
$N_{st} = t_d/\Delta t$
$N_t = t/\Delta t$

In the main text, three methods for performing the synaptic transformation are described. The first is explicit convolution using precalculation of the conductance waveform with storage. The second is explicit convolution involving no storage. The third is the differential or second-order method.

The method of convolution with precalculation requires an amount of computation proportional to

$$T_{computation} = N_{syn} N_{sp} T_c + N_{syn} N_{sp} N_{st} T_g \tag{9.45}$$

with additional storage proportional to $N_{syn} N_{st}$.

For explicit convolution without storage we have

$$T_{computation} = N_{syn} N_{sp} N_{st} T_c + N_{syn} N_{sp} N_{st} T_g \tag{9.46}$$

We can see that there is an additional factor of N_{st} in the first term (communication) while the second terms (calculation) are equivalent.

For the differential representation we have

$$T_{computation} = N_{syn} N_{sp} T_c + N_{ch} N_t T_s \tag{9.47}$$

In this formulation we see that the first term is as efficient as the convolution with precalculation without the storage overhead. The second term can be compared with the explicit convolution methods by looking at the factors N_{ch} versus N_{syn} and N_t versus $N_{st} N_{sp}$. Typically the number of synaptic targets or channels will be much less than the number of synapses N_{syn}. Additionally, factor N_t will be smaller than $N_{st} N_{sp}$ if there is overlap of the conductance intervals. Therefore, in general, the differential representation will be more computationally efficient than either of the explicit convolution methods.

As a sample calculation, we will examine a simulation of 100 cells each containing 5 synaptically activated channels. The simulation duration is 200 *msec* with $\Delta t = 1$ *msec*. All synaptic conductances have duration of 10 *msec*.

N_{syn}	10000 synapses	N_{ch}	500 channels
N_{st}	10 steps	N_t	200 steps
T_c	0.02 msec/synapse	T_s	0.1 msec/channel
T_g	0.005 msec/synapse		

for $N_{sp} = 20$

	communication	calculation	total
T_1	4 sec	10 sec	14 sec
T_2	40 sec	10 sec	50 sec
T_3	4 sec	10 sec	14 sec

for $N_{sp} = 100$

		calculation	total
T_1	20 sec	50 sec	70 sec
T_2	200 sec	50 sec	250 sec
T_3	20 sec	10 sec	30 sec

for $N_{sp} = 100$ and $\Delta t = 0.1$, which gives $N_{st} = 100$, and $N_t = 2000$.

	communication	calculation	total
T_1	20 sec	500 sec	520 sec
T_2	2000 sec	500 sec	2500 sec
T_3	20 sec	100 sec	120 sec

where T_1 is the computation time required for convolution with pre-calculation, T_2 is for explicit convolution, and T_3 is for the differential representation.

Appendix 9.D: Sample Calculation for Evaluation of Output Representation

In the following discussion the term "source" will refer to cells which are generating output while "target" will refer to cells receiving input.

N_s^s = the number of simulated cells in the source region
N_s^a = the actual number of cells in the source region to be simulated
N_t^a = the actual number of cells in the target region to be simulated
N_c = the number of connections on a target cell from cells in the source region of the actual network

What we wish to obtain is a simple measure of the appropriateness of the single-spike representation versus the spatially averaged output

representation as discussed in the main text. This measure is based on an estimation of the number of connections between a cell in the target region and cells within the representative source region.

The total number of connections made in the target region is given by

$$T_c = \sum_{\lambda}^{N_t^a} N_c(\lambda) \tag{9.48}$$

In the case of uniformly distributed connections $T_c = N_c N_t^a$
The number of connections made per source cell is

$$C_s = \frac{N_c N_t^a}{N_s^a} \tag{9.49}$$

The number of cells in the representative source region is

$$N_r = \frac{N_s^a}{N_s^s} \tag{9.50}$$

The estimated number of cells in the source region that project to a single target cell is given by

$$N_p = \frac{C_s N_r}{N_t^a} = \frac{N_c}{N_s^s} \tag{9.51}$$

The measure of output representation can be summarized as

$N_p >$ spatial average approximation with N_p discrete levels
$N_p \leq 1$ single-cell approximation with connection sparsity equal to N_p

Therefore, for valid single-spike approximation of cell output

$$N_s^s \geq N_c \tag{9.52}$$

For example, in the simulations of piriform cortex, looking at connectivity between cells within the cortex we have $N_s^s = N_c = 10^3$, giving $N_p = 1$ Thus the scale of the piriform cortex simulations lies at the transition point between fully connected single-cell output and discrete-level spatial average output.

For small N_s the spatial average technique provides an estimate that is more sensitive, in a relative sense, to variability in output levels given variability in input levels. The continuous approximation for the output

level will be a function of N_p. As N_p increases the resolution or number of discrete levels that the averaged output can take increases, making a continuous or at least a higher resolution output desirable. Single-cell input and output parameters must take into account the continuous nature of the output. We will assume that the effect of the averaged output will be to activate a synaptic conductance change in the target cell consistent with the single-spike effect. The instantaneous value of conductance should reflect the expected value of the conductance given input from multiple sources. If the components of the input are assumed to be independent in time, then the expected value is simply the sum of the mean value of the individual conductance waveforms. This allows the conductance to be represented as a function of input amplitude alone. The assumption of independence is clearly a major simplification. The presence of local excitatory and inhibitory connectivity would indicate that cells in a region are not independent but are influenced by the structure of local circuitry. Yet both the single-spike and spatial-average approaches make implicit assumptions concerning the significance of local variability in the output of a region of cells. Unfortunately this issue cannot be resolved without increases in simulation size or complexity of local transformations, both of which require a deeper understanding of the structure and function of local circuitry.

Synchronous coactivation of cells within a source region reduces the independence of output activity. This has the effect of reducing the number of independent connections N_c on the target cells, thereby reducing the single-spike criterion N_p. In the extreme case of complete coactivation, which is the approximate effect of commonly used shock stimulation, $N_c = 1$ and the input can be safely reduced to a single fiber that has single-valued spike output.

Table 9.1: Model parameters for piriform cortex

t_r	absolute refractory period	10 $msec$
t_e	synaptic delay	0.8 msec
$t_{d(ff)}$	feedforward inhibitory delay	50 $msec$
τ_{Na}	excitatory conductance time constant	3 $msec$
τ_{Cl}	feedback inhibitory conductance time constant	10 $msec$
τ_K	feedforward inhibitory conductance time constant	50 $msec$
$G_{peak(Na)}$	peak excitatory conductance	50 nS
$G_{peak(Cl)}$	peak feedback inhibitory conductance	200 nS
$G_{peak(K)}$	peak feedforward inhibitory conductance	5 nS
r_m	membrane leakage resistance	100 $M\Omega$
c_m	membrane capacitance	100 pF
E_{Na}	excitatory equilibrium potential	55 mV
E_{Cl}	feedback inhibitory equilibrium potential	–65 mV
E_K	feedforward inhibitory equilibrium potential	–90 mV
E_m	resting membrane potential	–90 mV
ν_{LOT}	main afferent LOT velocity	7 m/s
ν_{col}	afferent collateral velocity	1.6 m/s
ν_{ros}	rostrally directed velocity	1.0 m/s
ν_{cau}	caudally directed velocity	0.5 m/s
ν_{inh}	inhibitory velocity	1.0 m/s

Multicompartmental pyramidal cell parameters

C_m	membrane capacitance	1 $\mu F/cm^2$
R_m	membrane resistance	2000 Ωcm^2
R_e	extracellular resistance	50 Ω/cm
R_a	intracellular resistance	50 Ωcm

Cellular dimensions

segment	length (μm)	diameter (μm)
apical Ia dendrites	100	1.5
superficial Ib dendrites	100	1.5
deep Ib dendrites	100	1.5
soma	30	30
basal dendrites	200	1.5